A single-bond approach to orientation-dependent interactions and its implications for liquid water

Thomas M. Truskett, Pablo G. Debenedetti,[a] and Srikanth Sastry[b]
Department of Chemical Engineering, Princeton University, Princeton, New Jersey 08544

Salvatore Torquato
Princeton Materials Institute, Princeton University, Princeton, New Jersey 08544 and Department of Civil Engineering and Operations Research, Princeton University, Princeton, New Jersey 08544

(Received 15 March 1999; accepted 11 May 1999)

A simple model of an associating fluid is proposed that accounts for the fact that hydrogen bonds are highly directional and favor the formation of locally open structures. The resulting analytical equation of state reproduces the distinguishing thermodynamic features of liquid water. In contrast to previous models in which the relationship between bonding and bulk density is assumed *a priori*, the extent of hydrogen bonding is derived in the present work from a simple microscopic model. Furthermore, by altering the parameters which control the geometric constraints on bonding, the model is able to exhibit the two thermodynamically consistent scenarios that can explain the observed behavior of supercooled liquid water, namely the two-critical-point and singularity-free scenarios. This suggests that the two scenarios are closely related through subtle features of the hydrogen-bond geometry. © *1999 American Institute of Physics.* [S0021-9606(99)50230-4]

I. INTRODUCTION

Physical models have significantly advanced our understanding of the liquid state. Progress is perhaps most evident in the case of dense, simple liquids which comprise atoms that interact through spherically-symmetric potentials. A key feature of these systems is that the local structure, at least in the vicinity of the triple point, is dominated by repulsive interactions. In contrast, attractive forces play a relatively minor role in the structuring of molecules and can be treated as contributing a uniform background potential that confers the liquid its cohesive strength. This simple van der Waals picture set the foundation for modern perturbation theories, which accurately describe the thermodynamic properties of simple atomic liquids.[1–3]

A qualitatively different picture is expected to hold for the so-called *associating* liquids. In contrast to the orientationally smooth attractions characteristic of simple fluids, the attractive forces relevant to association are strongly orientation-dependent. The most common associative interaction is the hydrogen bond. Such bonds are strong, directional attractions that exist between an electronegative atom and a hydrogen that is covalently bonded to another molecule. The directionality of this interaction constrains the orientations of participating molecules and, consequently, favors the formation of open structures. This is particularly notable in water, a substance which can form space-filling, open networks in which each molecule is hydrogen bonded to its four nearest neighbors.[4] Ordinary ice is perhaps the best-known example of such a tetrahedrally-coordinated network, with each molecule acting as a hydrogen donor towards two neighbors and as an acceptor towards the other two. Silica is another classic example of a substance which forms a low-density network of strong, directional bonds.[5,6]

In the liquid phase, hydrogen bonds promote ordered (low entropy) and open (low density) structures that are necessarily both localized and transient. These bonded structures are energetically favorable and thus increase appreciably in size as the liquid is cooled towards its freezing point. This has a pronounced effect on the bulk thermodynamic behavior of liquid water.[7] For instance, the familiar density maximum that occurs at 4 °C signals that the fluid expands when cooled isobarically below this temperature. If the liquid is cooled below its freezing point without crystallization (supercooled), many of its physical properties exhibit anomalous behavior. Examples include large increases in isothermal compressibility κ_T, isobaric heat capacity c_P, and in the magnitude of the thermal expansion coefficient α_P upon cooling, and an increase in molecular mobility as the liquid is compressed isothermally.[8–12]

At even lower temperatures, amorphous solid (glassy) water is known to exhibit a phenomenon known as *polyamorphism*[13–15] in which two different forms, termed low-density amorphous ice (LDA) and high-density amorphous ice (HDA), are separated by a seemingly first-order transition. Evidence suggests that liquid water and its glassy phases are both thermodynamically and structurally continuous,[16–18] implying that the sharp change in density that accompanies the transformation from LDA into HDA is the structurally arrested manifestation of an underlying liquid–liquid transition that is metastable with respect to crystallization. This interpretation is commonly referred to as the *two-critical-point* scenario because it attributes the anomalies of supercooled water to the presence of a second critical point, where the first-order phase transition between LDA and HDA terminates. Results from computer

[a]Electronic mail: pdebene@princeton.edu
[b]Permanent address: Jawaharlal Nehru Center for Advanced Scientific Research, Bangalore 560064, India.

simulations and theoretical calculations are consistent with this scenario.[19–25]

A second thermodynamic scenario for liquid water has been proposed in which the large increases in the thermodynamic response functions occur in the absence of any assumed low-temperature singularity.[26–30] This so-called *singularity-free* scenario is related to the thermodynamic requirement that the increase in isothermal compressibility upon supercooling is inseparable from the existence of a negatively-sloped locus of density maxima in the $P-T$ plane,[28] a feature that water exhibits over a broad range of temperatures and pressures. The experimentally observed continuity between liquid and glassy water[16–18] rules out the retracing spinodal hypothesis,[31] the first thermodynamically consistent scenario proposed to explain supercooled water's anomalies. The present understanding of liquid and glassy water's low-temperature properties, in other words, admits two thermodynamically consistent interpretations, the two-critical-point and singularity-free scenarios.

An important feature of both hypotheses for supercooled water is their ability to describe the distinguishing thermodynamic features of liquid water under experimentally accessible conditions. Specifically, it has been shown that the experimentally observed locus of density maxima and locus of compressibility minima can be reproduced by either thermodynamic scenario.[32,29] Furthermore, both the two-critical-point and singularity-free hypotheses predict that the locus of density maxima changes slope in the negative pressure region of the $P-T$ plane to avoid the superheated liquid spinodal, a feature that has been observed in simulations of liquid water.[19]

Since liquid water cannot be studied experimentally below its homogeneous nucleation temperature (ca. $-42\,^{\circ}\mathrm{C}$ at one atmosphere), the hypothesis of a liquid–liquid transition has not been unambiguously verified. Here, simple models can provide insight into the possible global phase behaviors that can underlie the experimentally observed anomalies; elucidate the connection between microscopic details of hydrogen bonding and the resulting thermodynamics; and perhaps suggest experiments that can distinguish between the two scenarios. In this spirit, Poole *et al.*[32] derived an extended van der Waals equation of state that incorporates the effects of hydrogen bonding. Their approach was especially insightful because it demonstrated that the superposition of a hydrogen-bonding term onto the van der Waals free energy results in an equation of state capable of qualitatively reproducing water's anomalies. This work has been recently extended by Jeffery and Austin[33] in order to generate a quantitative equation of state for liquid water.

A key feature of the work of Poole and co-workers,[32] of its recent extension by Jeffery and Austin,[33] and of the related lattice model of Borick *et al.*[34] is the *a priori* assumption of the form of the relationship between the bulk density and the fraction of molecules that participate in hydrogen bonds. The nature of this approximation precludes establishing a connection between the microscopic details of bonding geometry and the resulting thermodynamic behavior. In the present work, we address this important issue by deriving the relationship between the extent of hydrogen bonding and the thermodynamic behavior by *solving* a simple microscopic model.

Commonly, associative interactions such as the hydrogen bond are treated within the theoretical framework of either a chemical or a perturbation theory. In the chemical theory approach, hydrogen bonds result from the formation of new molecular complexes such as dimers, timers, etc. Thus, the equation of state can be determined from solving the material balances and equilibrium conditions for the various complexed species.[35] Thermodynamic perturbation theories for water, on the other hand, are generally extensions of Wertheim's statistical mechanical formalism for associating fluids[36,37] and require an orientation-dependent potential as an input. Typical intermolecular potentials used in conjunction with Wertheim's theory are primitive models that consist of a repulsive core and multiple interaction sites that mimic the directional interactions characteristic of liquid water.[38] Both the chemical theory and thermodynamic perturbation theories have been relatively successful in describing water's vapor–liquid coexistence and the equation of state in the supercritical region.[35,39–42] However, an important deficiency of modern theories of association is their inability to reproduce many of the distinguishing thermodynamic features of stable and supercooled liquid water, including density maxima, compressibility minima, and anomalous increases in the response functions. This is due, in part, to the absence of a strong correlation between hydrogen bonding, loss of orientational entropy, and the existence of a low-density environment in the vicinity of a hydrogen bond.

An exception to this rule is the perturbation theory of Dahl and Andersen[43] which considers a sophisticated model potential with orientation-dependent interactions of varying attractive strength. The resulting approximate cluster theory permits numerical evaluation of the thermodynamic properties, which are found to be in good qualitative agreement with experimental trends.

In this work, we present a model that incorporates the known local correlation between low density, low energy, and low entropy in the vicinity of a hydrogen bond. This results in a simple analytical equation of state capable of describing with surprising accuracy the thermodynamics and phase behavior of supercooled liquid water. We consider the simplest case of a fluid with strongly directional interactions. Specifically, the fluid consists of molecules that can form at most a single hydrogen bond. The model and statistical mechanical development are presented in Sec. II. In Sec. III we use the model to calculate the thermodynamics and phase behavior and discuss the connection to water. In Sec. IV we present some concluding remarks.

II. MODEL FORMULATION

Owing to the importance of hydrogen bonding in our model, it is natural to begin with a microscopic description of the *geometric criteria* for the formation of a hydrogen bond. These criteria are designed to mimic the minimal features of hydrogen bonds in liquid water, namely, the molecules involved must possess mutually favorable orientation (low orientational entropy), and an open, low-density envi-

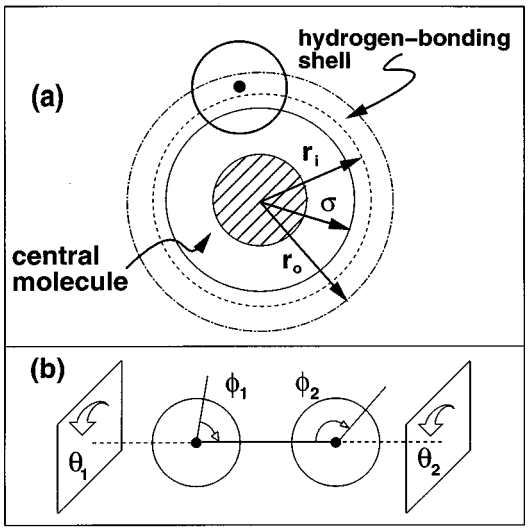

FIG. 1. The microscopic model of a fluid with orientation-dependent interactions. (a) Molecules have a hard core of diameter σ, and are therefore surrounded by an exclusion sphere of radius σ, within which the center of no other molecule can penetrate. In order to form a hydrogen bond, a central molecule must be surrounded by an empty cavity of radius r_i (here $r_i \approx \sigma$), and a second molecule must be inside its hydrogen bonding shell $r_i \leqslant r \leqslant r_0$. (b) In addition, the two participating molecules must be properly oriented, with their bonding directions pointing towards each other ($\phi_1, \phi_2 \leqslant \phi^*$), regardless of the value of θ_1 and θ_2. The presence of additional molecules inside the hydrogen bonding shell weakens an existing bond.

ronment must exist in the vicinity of the bond. These basic physical attributes of the hydrogen bond are modeled as follows (see Fig. 1):

(1) One of the two participating molecules must have a cavity of radius r_i, empty of any molecular centers, surrounding it. We term this the *central molecule* of the pair.
(2) The pair must be separated by a distance r that lies within the *hydrogen-bonding shell* of the central molecule, with $r_i \leqslant r \leqslant r_0$.
(3) The pair must exhibit mutually favorable orientation, $\phi_1, \phi_2 \leqslant \phi^*$.
(4) The presence of additional molecules in the hydrogen-bonding shell ''crowds'' and thereby weakens the existing bond. We assign a strength $-\epsilon_{\max}$ to a hydrogen bond and a penalty ϵ_{pen} for each nonbonding molecule in the hydrogen-bonding shell. In this study, we take $-\epsilon_{\max} = -23$ kJ/mol and $\epsilon_{\text{pen}} = 3$ kJ/mol. It follows that if more than seven nonbonding molecules are contained in the hydrogen-bonding shell, the central molecule is not available for bonding.

Each of these criteria is designed to model, albeit in a rudimentary fashion, specific features of the hydrogen-bond interaction. For instance, the requirement of a cavity of radius r_i surrounding the central molecule promotes a low-density, open environment in the vicinity of the bonded pair. Criterion (2) defines the largest allowable separation r_0 for molecular centers participating in a hydrogen bond. Indeed, the shell ($r_i \leqslant r \leqslant r_0$) physically represents the width of the distribution of bond lengths in the model substance. For perspective, typical bond lengths in $(H_2O)_2$ measured in the vapor phase (2.98 Å) are roughly 8% larger than the observed distance in ice.[4] Criterion (3) constrains the bonding sites on each molecule to lie within an angle ϕ^* of the line connecting molecular centers. The magnitude of ϕ^* determines the freedom of alignment between molecular sites, and thus is necessarily related to the reduction of orientational entropy upon bonding. As will be demonstrated, minor alterations in the geometric ''librational'' and ''vibrational'' bonding constraints, as defined by (r_i, r_0, ϕ^*), can result in dramatic changes in the macroscopic phase behavior of the system. Criterion (4) prescribes the dependence of the hydrogen-bond energy $-\epsilon_j$ on its local structural environment,

$$-\epsilon_j = -\epsilon_{\max} + (j-1)\epsilon_{\text{pen}}, \tag{2.1}$$

where $j-1$ is the number of nonbonded molecules in the hydrogen-bonding shell of the central molecule. This crowding rule is a simple model for the fact that hydrogen bonding is a many-body interaction, i.e., the presence of nonbonding neighbors can severely disrupt the electronic structure of the bonded pair. Certainly, these criteria oversimplify the microscopic details of the hydrogen bond. For instance, this coarse description will not promote many of the structural details characteristic of liquid water, such as local tetrahedral ordering. Nevertheless, the model provides a framework within which the effect of simple directional bonding on the thermodynamics of a fluid can be studied analytically.

Connection between microscopic forces and equilibrium thermodynamics is established through the canonical partition function Q,[44]

$$Q(N,V,T) = \left(\frac{1}{N!\Lambda^{3N}}\right) \int \int d\mathbf{r}^N d\mathbf{\Omega}^N \exp(-\beta\Phi), \tag{2.2}$$

from which the Helmoltz free energy is obtained, $A = -kT \ln Q(N,V,T)$. Here, $\beta = 1/kT$, k is Boltzmann's constant, T is the temperature, N is the number of molecules, and V is the volume. For a monatomic species, Λ is the familiar thermal wavelength. For polyatomic molecules, Λ is generalized to include contributions from relevant internal degrees of freedom; however, it exhibits no pressure or density dependence. The multidimensional integral over the set of $5N$ scalar variables, $\{r_1, \ldots, r_{3N}\}$ and $\{\Omega_1, \ldots, \Omega_{2N}\}$ defining the instantaneous position and orientation of each molecule, is the configurational contribution to the partition function. Note that an axis of symmetry leaves two orientational and three translational degrees of freedom per molecule. Φ is the potential energy and is a complex function of the positions and orientations.

We decompose the potential energy into three contributions,

$$\Phi = \Phi_{\text{HS}} + \Phi_{\text{disp}} + \Phi_{\text{HB}}, \tag{2.3}$$

which represent hard-sphere, dispersion, and hydrogen-bonding interactions, respectively. We model the hard-sphere interaction by assigning an impenetrable core of diameter σ to each molecule. The dispersion interaction plays a relatively minor role in the structuring of molecules, and

thus it is often modeled by a uniform, attractive background potential. We invoke this mean-field approximation by replacing the dispersion term with an effective potential energy $-\rho a$ per molecule ($\rho = N/V$). The resulting partition function may be written

$$Q(N,V,T) \approx \left(\frac{1}{N!\Lambda^{3N}}\right) \exp(N\beta\rho a) \int\int d\mathbf{r}^N d\mathbf{\Omega}^N \times \exp[-\beta(\Phi_{\mathrm{HS}} + \Phi_{\mathrm{HB}})]. \tag{2.4}$$

The integrals appearing in this relation may be rewritten as

$$\int\int d\mathbf{r}^N d\mathbf{\Omega}^N \exp[-\beta(\Phi_{\mathrm{HS}} + \Phi_{\mathrm{HB}})] = \left[\int d\mathbf{r}^N \exp(-\beta\Phi_{\mathrm{HS}})\right] \int d\mathbf{\Omega}^N \langle \exp(-\beta\Phi_{\mathrm{HB}})\rangle_{\mathrm{HS}}. \tag{2.5}$$

Note that this transformation is exact. Focusing on the right-hand side of the equality, the first integral in the product represents the configurational partition function for the hard-sphere fluid. In the second integral, the notation $\langle \exp(-\beta\Phi_{\mathrm{HB}})\rangle_{\mathrm{HS}}$ indicates that the thermodynamic average of $\exp(-\beta\Phi_{\mathrm{HB}})$ is to be taken in the hard-sphere ensemble. This implies sampling all possible configurations of N hard spheres at a given density, and calculating, for each such configuration, the value of $\exp(-\beta\Phi_{\mathrm{HB}})$ by ''turning on'' the hydrogen bonds with fixed molecular orientation. The integral is then taken over all possible sets of orientations.

If we assume the simplest approximation for the available volume in the hard-sphere fluid $[V-Nb]$, exact only in one dimension, then the partition function becomes

$$Q(N,V,T) = \left(\frac{1}{N!\Lambda^{3N}}\right) (V-Nb)^N \exp(N\beta\rho a) \int d\mathbf{\Omega}^N \times \langle \exp(-\beta\Phi_{\mathrm{HB}})\rangle_{\mathrm{HS}}. \tag{2.6}$$

We have explored the use of more accurate excluded volume approximations, such as the Carnahan–Starling equation of state[45] or Padé approximant fits to simulation data. They all produce qualitatively similar results.

For a general random variable x, we note the familiar cumulant expansion[46]

$$\langle \exp(cx)\rangle = \exp\left[c\langle x\rangle + \frac{c^2}{2!}(\langle x^2\rangle - \langle x\rangle^2) + \cdots\right]. \tag{2.7}$$

We determine the hard-sphere contribution to Eq. (2.6) approximately by neglecting fluctuations. Explicitly, we neglect second and all higher order cumulants

$$\langle \exp(-\beta\Phi_{\mathrm{HB}})\rangle_{\mathrm{HS}} \approx \exp\langle -\beta\Phi_{\mathrm{HB}}\rangle_{\mathrm{HS}} = \exp\left[N\beta\sum_{j=1}^{8} p_j\epsilon_j\right], \tag{2.8}$$

where this term still depends on the orientation of each individual molecule. Specifically, if one of the j molecules in the hydrogen-bonding shell shares correct mutual orientation with the central molecule then a hydrogen bond of strength $-\epsilon_j = [-23 + 3(j-1)]$ kJ/mol is formed. On the other hand, if none of the j molecules shares correct mutual orientation with the central molecule then $\epsilon_j = 0$. Here, p_j represents the probability that, in a hard-sphere fluid at the density of interest, a given hard sphere has a cavity of radius r_i surrounding it and that j other sphere centers lie within its hydrogen-bonding shell (Fig. 1). This is tantamount to stating that the hard sphere meets the positional (if not the orientational) requirements for hydrogen-bonding to one of its j neighbors.

Implicit in Eq. (2.8) is the assumption that central molecules are never in a position to bond to one another. This is a reasonable scenario at high densities, where central molecules (which must have a cavity of radius r_i surrounding them) are scarce. It is further assumed that a given molecule can only exist in the hydrogen-bonding shell of one central molecule at a time. From an energetic viewpoint, an optimal set of orientations for the molecules would result in a configuration containing a total of Np_j bonds of energy $-\epsilon_j (1 \leqslant j \leqslant 8)$. Together with the physical constraint of one hydrogen bond per molecule, this allows for the explicit evaluation of the orientational integrals appearing in the partition function. Recalling that ϵ_j is zero except when the central molecule (with orientation θ_1, ϕ_1) and one neighbor (with orientation θ_i, ϕ_i) are mutually aligned ($\phi_1, \phi_i \leqslant \phi^*$) we have

$$\begin{aligned}\int d\mathbf{\Omega}^N \exp\left(N\beta\sum_{j=1}^{8} p_j\epsilon_j\right) &= (4\pi)^{N\{1-\sum_{k=1}^{8}(k+1)p_k\}} \prod_{j=1}^{8} \left[\int_0^{2\pi} d\theta_1 \cdots \int_0^{2\pi} d\theta_{j+1} \times \int_0^{\pi} d\phi_1 \sin(\phi_1)\cdots \times \int_0^{\pi} d\phi_{j+1} \sin(\phi_{j+1}) \exp(\beta\epsilon_j)\right]^{Np_j} \\ &= (4\pi)^N \prod_{j=1}^{8} f_j^{Np_j},\end{aligned} \tag{2.9}$$

where f_j is given by

$$f_j = \left[1 + \frac{j}{4}(1-\cos\phi^*)^2(\exp\{\beta\epsilon_j\} - 1)\right], \tag{2.10}$$

and ϕ^* is defined in Fig. 1. The resulting partition function reads

$$Q(N,V,T) = \left(\frac{1}{N!\Lambda^{3N}}\right) (V-Nb)^N \exp(N\beta\rho a)(4\pi)^N \times \prod_{j=1}^{8} f_j^{Np_j}. \tag{2.11}$$

Differentiation yields the pressure

$$P = kT\left(\frac{\partial \ln Q(N,V,T)}{\partial V}\right)_{T,N} = \frac{\rho kT}{1-\rho b} - a\rho^2 - \rho^2 kT \sum_{j=1}^{8} \left(\frac{\partial p_j}{\partial \rho}\right)_T \ln f_j, \tag{2.12}$$

which is simply the van der Waals equation of state plus a hydrogen-bonding contribution. It is useful to relate the ex-

cluded volume per particle b to the hard-core diameter σ. We require the pressure to diverge at the familiar random close packing density

$$0.64b = \frac{\pi\sigma^3}{6}, \tag{2.13}$$

where the spheres occupy 64% of the volume.

To complete the picture, we need to obtain an expression for p_j. Consider this quantity as a product of two probabilities

$$p_j = p(r_i,0)\cdot p(r_0,j/r_i). \tag{2.14}$$

The first quantity is the probability that a given sphere has a cavity of radius r_i, empty of other sphere centers, surrounding it. The second term is the conditional probability that there are exactly j particles in the sphere's hydrogen bonding shell ($r_i \leqslant r \leqslant r_0$), given that there is a empty cavity of radius r_i surrounding the central particle. The following rigorous expression for $p(r_i,0)$ can be derived:[47]

$$p(r_i,0) = \exp\left[-4\pi\rho\int_\sigma^{r_i} r^2 G(r)dr\right], \tag{2.15}$$

where $G(r)$ is called the *conditional pair-distribution function*, and $\rho G(r)$ is the concentration of sphere centers located a distance r away from a hard-sphere center, given that there are no sphere centers closer than r. This quantity plays an important role in the scaled-particle theory (SPT),[48] and more generally, in the *statistical geometry* of liquids, which has contributed many exact relations that bound the thermodynamic properties of hard-particle systems.[49–53] In the spirit of SPT, Torquato[47] derived an analytical approximation for $G(r)$,

$$\begin{aligned} &G(r) = 0 \quad r < \sigma, \\ &G(r) = a_0 + \frac{a_1}{(r/\sigma)} + \frac{a_2}{(r/\sigma)^2} \quad r \geqslant \sigma, \end{aligned} \tag{2.16}$$

with

$$\begin{aligned} a_0 &= 1 + 4\eta G(\sigma), \\ a_1 &= \frac{3\eta - 4}{2(1-\eta)} + 2(1-3\eta)G(\sigma), \\ a_2 &= \frac{2-\eta}{2(1-\eta)} + (2\eta - 1)G(\sigma), \\ G(\sigma) &= \frac{1-\eta/2}{(1-\eta)^3}, \end{aligned} \tag{2.17}$$

where the packing fraction η is given by $\rho(\pi\sigma^3/6)$. Here, we choose the simple approximation

$$p(r_0,j/r_i) = \frac{1}{j!}\left(4\pi\rho\int_\sigma^{r_0} r^2 G(r)dr\right)^j \times \exp\left[-4\pi\rho\int_\sigma^{r_0} r^2 G(r)dr\right]. \tag{2.18}$$

This expression is appealing because it approaches the exact description in the dilute limit when the cavity surrounding the central molecule is small ($\eta \to 0$, $r_i \to \sigma$). Furthermore, we have found that the expression is quite accurate for low densities and captures many qualitative features of the correlations at higher densities.

This completes the development of a simple analytical theory for the thermodynamics of a hydrogen-bonding fluid. In the next section, we investigate the the thermodynamics and phase behavior of the theory and discuss connections with supercooled liquid water.

III. RESULTS AND DISCUSSION

Notice that the model equation of state (2.12) depends on a total of 7 parameters that can be varied independently ($r_i, r_0, \epsilon_{\max}, \epsilon_{\text{pen}}, \phi^*, \sigma, a$). In the present work, we present results obtained by varying the three parameters that describe the hydrogen-bond geometry (r_i, r_0, ϕ^*), while the remaining parameters ($\epsilon_{\max}, \epsilon_{\text{pen}}, \sigma, a$) were fixed. The magnitude of the maximum hydrogen-bond strength $\epsilon_{\max}$ and the hard-core diameter σ were set at the physically reasonable values of 23 kJ/mol and 3.11 Å, respectively. Recall that the crowding penalty ϵ_{pen} was set to 3 kJ/mol per nonbonding molecule in the hydrogen-bonding-shell. The dispersion interaction a was chosen to be 0.269 $\text{Pam}^6\,\text{mol}^{-2}$, which essentially fixes the vapor–liquid critical point at the correct experimental value of 647 K. Due to the simplified treatment of the dispersion interaction, the vapor–liquid critical density obtained ($\rho_c = 0.41\ \text{g/cm}^3$) is an overestimation of water's true critical point density ($\rho_c = 0.328\ \text{g/cm}^3$).

Since only three parameters are varied in this study, a simple protocol was developed to generate phase diagrams. Specifically, we freely varied one of the three parameters (r_i, r_0, or ϕ^*) within reasonable physical constraints, e.g., $\sigma \leqslant r_i \leqslant r_0$. The other two parameters were used to fix the (1 bar) density maximum at 4 °C and 1 g/cm^3.

Figure 2 shows that Eq. (2.12) can generate a phase diagram consistent with the two-critical-point scenario proposed for liquid water. Note the liquid–liquid transition that occurs at low temperature and high pressure. Consistent with the behavior of liquid water, the fluid expands upon isobaric cooling ($\alpha_p < 0$) over a large range of temperatures and pressures. This region of negative thermal expansion is enclosed by the locus of extrema in density (temperature of maximum/minimum density, TMD). Also shown is the locus of extrema in compressibility (temperature of extrema in compressibility, TEC), which bounds the region in which the isothermal compressibility κ_T increases upon isobaric cooling. As is required by thermodynamic consistency,[28] the TEC intersects the TMD when the latter attains infinite slope in the $P-T$ plane.

It is important to note that the model predictions of a locus of density maxima and a locus of compressibility minima are consistent with the known thermodynamic behavior of water. Furthermore the predicted change of slope of the TMD in the negative pressure region has also been observed in computer simulations of liquid water.[19]

Although the vapor–liquid and the liquid–liquid transitions are similar in shape in the temperature–density projection, there are some important differences. To illustrate one distinguishing feature, Fig. 2(a) includes three curves of con-

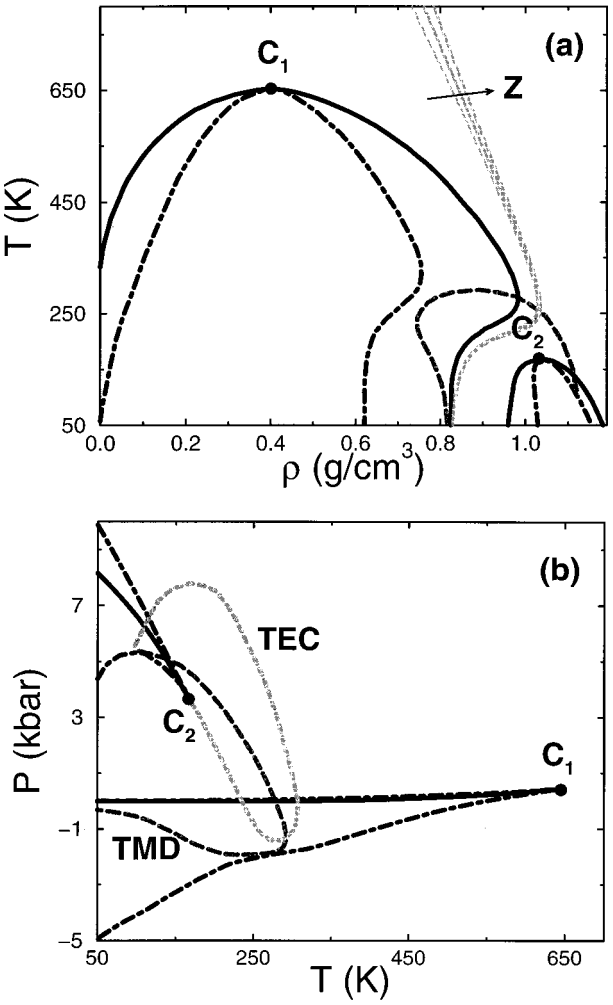

FIG. 2. Calculated phase behavior in the two-critical-point scenario. The model parameters are $\phi^*=0.175$ rad, $r_i=1.01\sigma$, $r_0=1.04\sigma$. Other parameters are given in the text. C_1 and C_2 are the the vapor–liquid and liquid–liquid critical points, respectively. Coexistence curves (dark solid), spinodal curves (dotted–dashed), and the locus of density extrema (TMD, dark dashed) are shown. The coordinates of C_2 are as follows: $P_C=3.7$ kbar, $T_C=167$ K, $\rho_C=1.04$ g/cm^3. (a) Temperature-density projection. Also shown are three curves of constant compressibility factor Z ($Z=0.9$, 1, 1.1; light, solid curves appearing in the diagram). (b) Pressure-temperature projection. The light dashed line is the locus of compressibility extrema (TEC) discussed in the text.

stant Z ($Z=0.9$, 1.0, and 1.1, respectively), where $Z=\beta P/\rho$ is the compressibility factor. The line $Z=1$ is a useful reference on the temperature–density projection because it effectively divides the phase diagram into regions where either repulsive ($Z>1$) or attractive forces ($Z<1$) make the predominant contribution to the pressure. In general, repulsive forces increase by heating or compression, hence the $Z=1$ locus is negatively-sloped for most fluids. Note the different behavior for water in the region $\alpha_P<0$. The locus of vapor–liquid coexistence, as is well-known, lies entirely within the $Z<1$ portion of the phase diagram, indicating that the transition is driven by attractive interactions. It is worth noting that, in contrast to the vapor–liquid transition, the liquid–liquid transition is dominated by repulsive contributions to the virial. Furthermore, the locus of phase coexistence for the liquid–liquid transition is negatively-sloped in the pressure–temperature projection of the phase diagram, indicating that the high-density liquid phase has a higher entropy than the low-density liquid phase.

Figures 3(a) and 3(b) show the behavior of the molar entropy s and the molar internal energy u in the two-critical-point scenario as the fluid is compressed through the liquid–liquid transition along the 100 K isotherm. As is the case in the van der Waals fluid, compression at low densities results in a monotonic decrease in the entropy and the internal energy. However, further compression causes the slope of the entropy to change in sign, corresponding to a change in the sign of the thermal expansion coefficient, followed by appreciable increases in both the entropy and the internal energy. Thus, the Helmoltz free energy ($u-Ts$) becomes double-welled at high density, and a second phase transition appears, as a consequence of the anomalous increase in entropy and energy upon compression. Note the contrast with the more common van der Waals-type behavior.

The aforementioned interplay between energy and entropy can be understood in terms of the extent of hydrogen bonding in the system. Figure 3(c) shows the fractional hydrogen-bonding energy f_{HB} plotted vs density ρ as calculated from the microscopic model. Here $f_{\mathrm{HB}}=u_{\mathrm{HB}}/u_{\mathrm{HB,ground}}$ is the ratio of the actual to the maximum (absolute value) possible hydrogen-bonding energy ($u_{\mathrm{HB,ground}}=-10.99$ kJ/mol for the set of parameters given in Fig. 2). The fractional hydrogen-bonding energy has an asymmetric density dependence about an optimal, temperature-dependent hydrogen-bonding density. As the fluid is compressed from low density, the extent of hydrogen bonding slowly increases. However, further compression of the bonded (low-energy) and ordered (low-entropy) structures results in a rapid decline in hydrogen bonding, indicating that the liquid–liquid transition shown in Fig. 2 is an equilibrium between an essentially open, bonded fluid and a densely-packed nonbonded fluid. The coexisting phases at 100 K are shown in Fig. 3(c).

Figure 4 shows the singularity-free behavior. Note the disappearance of the liquid–liquid transition, but the persistence of other distinguishing thermodynamic features, including the loci of density and compressibility extrema and the nonmonotonic liquid branch of the vapor–liquid coexistence curve.

Remarkably, the model predicts that the change of thermodynamic scenarios results from only modest differences in the parameters controlling the hydrogen-bond geometry; the set of geometric parameters is given by ($\phi^*=0.175$ rad, $r_i=1.01\sigma$, $r_0=1.04\sigma$) and ($\phi^*=0.16$ rad, $r_i=1.005\sigma$, $r_0=1.03\sigma$) for the two-critical-point and singularity-free scenarios, respectively. The singularity-free scenario results from tightening the constraints for hydrogen bond formation, while maintaining the same physical values for the energy of a hydrogen bond. This clearly suggests that the two scenarios arise from the same microscopic physics.

Alterations in the bonding parameters have the expected effect on the thermodynamic properties in the supercooled region. Generally, tightening the width of the hydrogen-bonding shell r_0-r_i or the bonding angle ϕ^* causes the anomalous behavior to occur at progressively lower tempera-

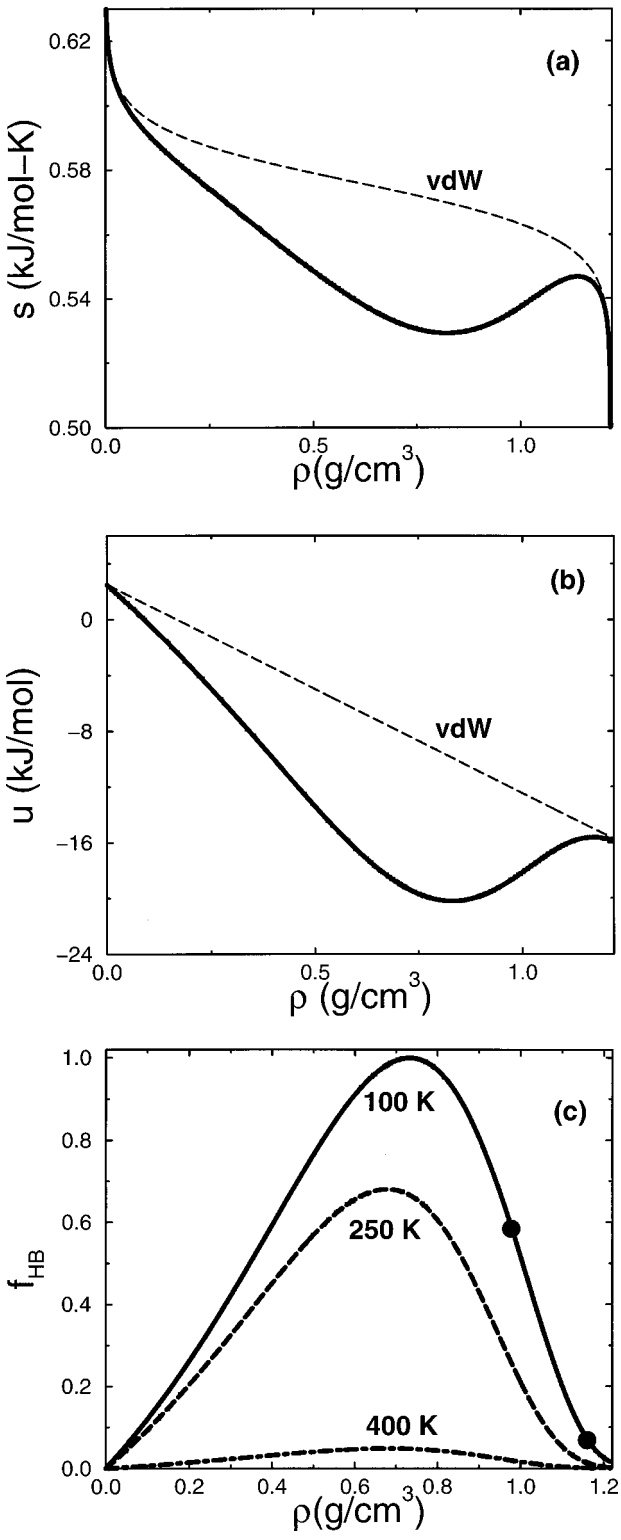

FIG. 3. (a) Molar entropy s and (b) molar internal energy u plotted vs density ρ along the $T=100$ K isotherm in the two-critical-point scenario. The full lines are model calculations for the fluid with orientation-dependent interactions (parameters given in Fig. 2) and the dashed lines are for the van der Waals fluid (hydrogen-bonding interactions ''turned off''). In contrast to the behavior of the van der Waals fluid, compression causes an increase in entropy and internal energy at high densities in the associating fluid. (c) Fractional hydrogen bonding energy f_{HB} (discussed in the text) plotted vs density ρ as calculated from the microscopic model. The filled circles indicate the hydrogen-bonding energy for the coexisting low-density and high-density liquid phases.

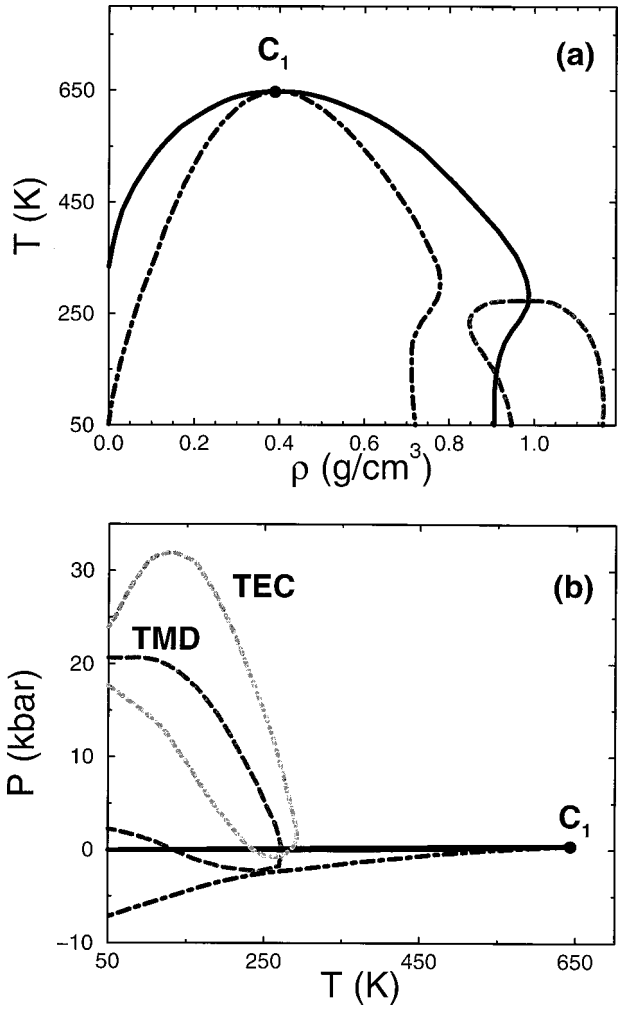

FIG. 4. Calculated phase behavior in the singularity-free scenario. The model parameters are $\phi^*=0.16$ rad, $r_i=1.005\sigma$, $r_0=1.03\sigma$. The legend and other parameters are unchanged with respect to those used in Fig. 2. (a) Temperature-density projection. (b) Pressure-temperature projection.

tures. Similar changes can be effected by increasing the penalty assigned to nonbonding neighbors ϵ_{pen}. If the minimum bond length r_i is decreased, with a fixed hydrogen-bonding shell width, the anomalies occur at progressively higher densities and pressures.

Interestingly, the prospect of a second critical point and related density anomalies in a pure fluid have been studied in the context of potentials that have a region of negative curvature or a shoulder in their repulsive core (so-called ''core-softened'' potentials).[54,55,25] This class of potentials promotes a local correlation between low-density and low-energy states without orientation-dependent interactions. As is shown in the Appendix, however, orientation-dependent interactions are necessary for reproducing density anomalies in the present theory.

It is well-known that water's thermodynamic response functions exhibit anomalous behavior in the supercooled region.[8,9] At atmospheric pressure κ_T, c_P, and the magnitude of α_P continue to increase down to the lowest temperatures at which such measurements have been made [-38 °C for c_P (Ref. 56)]. At higher pressures, the model predicts that these pronounced increases occur at progressively lower

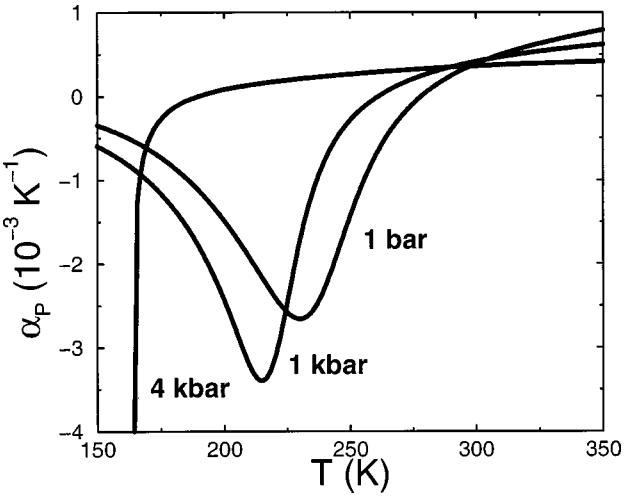

FIG. 5. Behavior of the thermal expansion coefficient α_P in the two-critical-point scenario.

temperatures. Figures 5 and 6 show the temperature dependence of α_P for several pressures in the two-critical-point and singularity-free scenarios, respectively. Note that the high-density liquid spinodal associated with the liquid–liquid immiscibility causes α_P to diverge at 4 kbar, while α_P remains finite down to the lowest calculable temperatures in the singularity-free scenario. The other thermodynamic response functions exhibit similar qualitative behavior.

Figure 7 illustrates the comparison of experimental measurements[10–12] of the thermal expansion coefficient α_P, the isothermal compressibility κ_T, and the molar heat capacity c_P with the corresponding theoretical predictions using Eq. (2). The theory yields a very good representation of the pronounced increases in compressibility and in the magnitude of the thermal expansion coefficient upon supercooling; however, the agreement with experimental data is consistently better for the set of parameters that gives rise to liquid–liquid immiscibility.

The agreement between experimental data and model predictions is less satisfying for the molar heat capacity c_P.

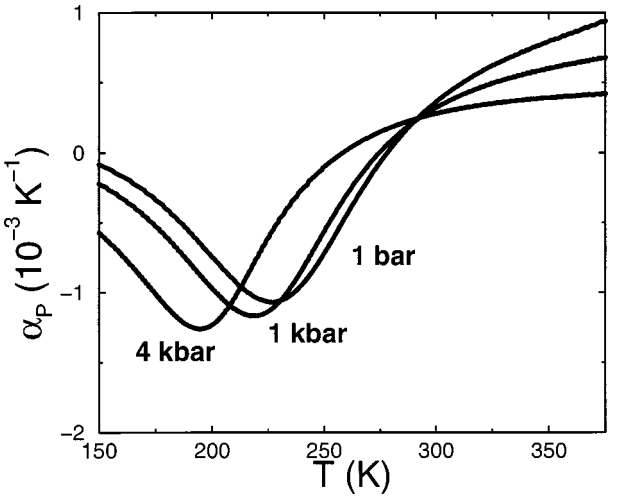

FIG. 6. Behavior of the thermal expansion coefficient α_P in the singularity-free scenario.

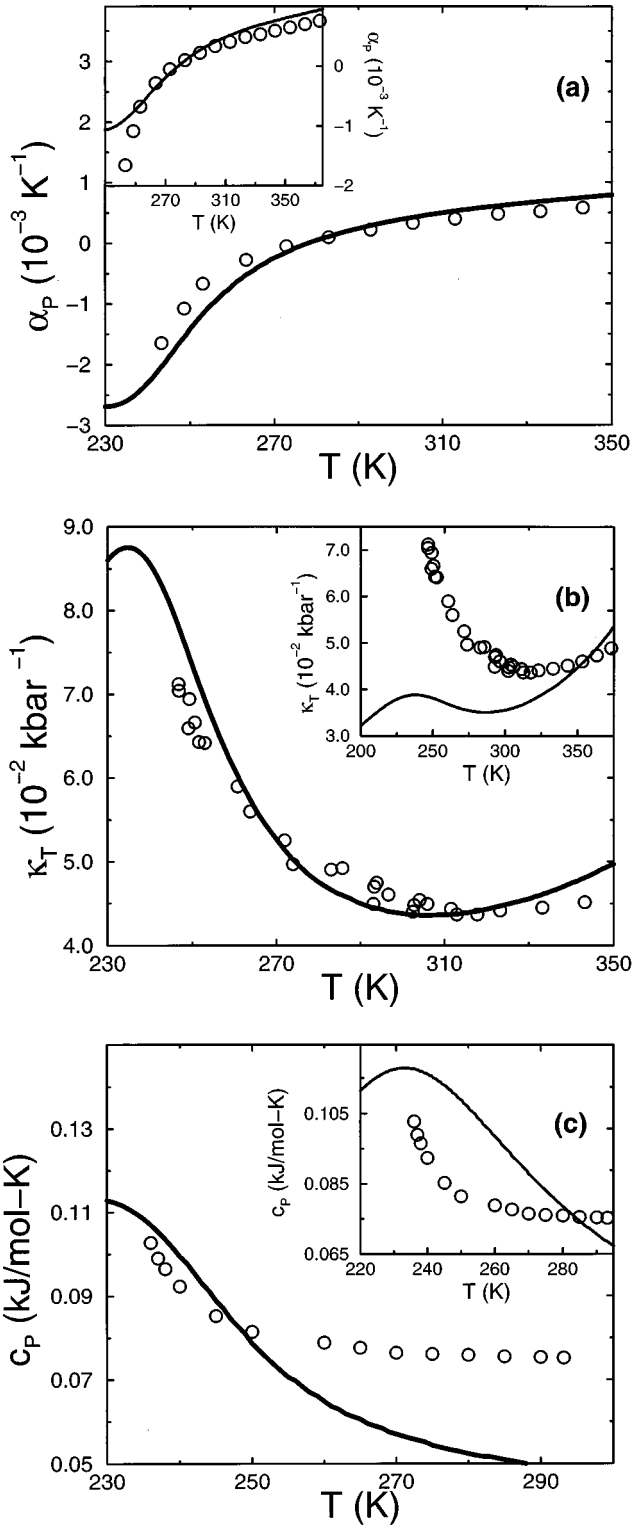

FIG. 7. Comparison of calculated and measured (Refs. 10–12) values of (a) the thermal expansion coefficient α_P, (b) the isothermal compressibility κ_T, and (c) the molar heat capacity c_P at 1 bar. Model parameters for the large plots are those which give rise to the two-critical-point scenario (Fig. 2). The insets show the corresponding comparison between experimental data and the model predictions in the singularity-free scenario (Fig. 3). Experimentally, a minimum in κ_T occurs at 46 °C (1 bar), while the model predicts the minimum to occur at 33 °C and 15 °C for the two-critical-point and singularity-free scenarios, respectively. A minimum in c_P for liquid water occurs at 34 °C (1 bar); the model predicts this broad minimum to occur at 96 °C and 127 °C for the two-critical-point and singularity-free scenarios, respectively. The parameters were set in both scenarios to capture the well-known density maximum occurring at 4 °C (1 bar).

In particular, both scenarios underestimate the magnitude of c_P in the high-temperature region. To understand why this is so, recall that c_P is related to the rate of change of entropy with respect to temperature at constant pressure [$c_P = T(\partial s/\partial T)_P$]. As should be expected, the grossly simplified orientational entropy of the single-bond model relative to water results in an underestimation of the molar heat capacity in the liquid state. We note, parenthetically, that although the model cannot capture the the behavior of the heat capacity quantitatively, the temperature range for the pronounced increase in heat capacity is captured satisfactorily by predictions of the two-critical-point scenario.

IV. CONCLUSIONS

We have presented the thermodynamic predictions of a simple analytic theory for an associating fluid. The ability of this model to describe density maxima, compressibility and specific heat minima, and sharp increases in response functions at low temperatures suggests that accounting for the correlation between hydrogen-bond formation, loss of orientational entropy, and the existence of a low-density local environment is key to understanding the thermodynamics of liquid water.[30] The incorporation of further structural details, such as local tetrahedral ordering, appear to be less important.

Depending on the values of the parameters that describe the hydrogen-bonding geometry, the model can generate either of the two thermodynamically consistent phase behaviors that can describe the anomalies in supercooled liquid water, namely the two-critical-point and the singularity-free scenarios. This suggests that the change from liquid–liquid immiscibility to singularity-free behavior is connected to subtle features of hydrogen bonding geometry. Given the high degree of metastability and imperfect equilibration of the LDA and HDA glassy phases, the model further highlights the difficulty of distinguishing experimentally between the two scenarios.

Perhaps the most important and challenging modification would be the addition of three more rigid bonding arms to the molecule. Such an improvement seems necessary for advancement toward a comprehensive theory of liquid water capable of describing both structure and thermodynamics.

ACKNOWLEDGMENTS

P.G.D. gratefully acknowledges support of the U.S. Department of Energy, Division of Chemical Sciences, Office of Basic Energy Sciences (Grant No. DE-FG02-87ER.13714), and of the donors of the Petroleum Research Fund, administered by The American Chemical Society. S.T. gratefully acknowledges the support of the U.S. Department of Energy, Office of Basic Energy Sciences (Grant No. DE-FG02-92ER14275). T.M.T. acknowledges the support of The National Science Foundation.

APPENDIX: REMOVING ORIENTATIONAL CONSTRAINTS ON THE HYDROGEN BOND

In order to understand the effect of bonding geometry on the global phase behavior and thermodynamics of this model, we remove the orientational dependence of the hydrogen bond. Specifically, we allow the central molecule to participate in $N_{\max}$ hydrogen bonds with molecules contained in its hydrogen-bonding shell [see Fig. 1(a)], independent of orientation. Using the familiar van der Waals form for the hard-sphere and dispersion terms, the resulting configurational partition function may be written

$$Q_{\mathrm{conf}} = (V-Nb)^N \exp(N\beta\rho a)\langle \exp(-\beta\Phi_{\mathrm{HB}})\rangle_{\mathrm{HS}}, \quad \text{(A1)}$$

where $\langle\cdots\rangle_{\mathrm{HS}}$ indicates an average in the hard-sphere ensemble. Once again, we assume that central molecules are not in a position to bond to each other and that molecules are only in one hydrogen-bonding shell at a time. Neglecting higher order in terms in the cumulant expansion of the Boltzmann factor, we have

$$\langle \exp(-\beta\Phi_{\mathrm{HB}})\rangle_{\mathrm{HS}} \approx \exp\langle -\beta\Phi_{\mathrm{HB}}\rangle_{\mathrm{HS}} = \exp\left[N\beta \sum_{j=1}^{N_{\max}} j p_j \epsilon_j \right]. \quad \text{(A2)}$$

As illustrated in Fig. 1(a), p_j is the probability that an empty cavity of radius r_i surrounds a given hard sphere, and that exactly j sphere centers are contained in its hydrogen-bonding shell. The hydrogen-bonding energy associated with this configuration of $j+1$ spheres is equal to $-j\epsilon_j$. The pressure is given by

$$P = kT\left(\frac{\partial \ln Q_{\mathrm{conf}}}{\partial V}\right)_{T,N} = \frac{\rho kT}{1-\rho b} - a\rho^2 - \rho^2 \sum_{j=1}^{N_{\max}} j\epsilon_j \left(\frac{\partial p_j}{\partial \rho}\right)_T, \quad \text{(A3)}$$

which is simply the van der Waals equation of state plus a density-dependent hydrogen-bonding term. Note that since the p_j refer to a hard-sphere fluid, the hydrogen-bonding term contains no temperature dependence.

To explore the thermodynamic implications of this equation of state, we look at the temperature dependence of the pressure along an isochore

$$\left(\frac{\partial P}{\partial T}\right)_\rho = \frac{\alpha_P}{\kappa_T} = \frac{\rho k}{1-\rho b} \geqslant 0, \quad \text{(A4)}$$

where $\alpha_P = (\partial \ln v/\partial T)_P$ is the isobaric thermal expansion coefficient and $\kappa_T = -(\partial \ln v/\partial P)_T$ is the isothermal compressibility. Since mechanical stability requires $\kappa_T > 0$, we see that the thermal expansion coefficient is always non-negative,

$$\alpha_P \geqslant 0, \quad \text{(A5)}$$

or equivalently, the fluid lacks densities anomalies. This suggests that orientation-dependent interactions are crucial for reproducing the qualitative features of liquid water.

[1] R. W. Zwanzig, J. Chem. Phys. **22**, 1420 (1954).
[2] J. A. Barker and D. Henderson, Rev. Mod. Phys. **48**, 587 (1976).
[3] D. Chandler, J. D. Weeks, and H. C. Andersen, Science **220**, 787 (1983).
[4] F. H. Stillinger, Science **209**, 451 (1980).
[5] M. Grimsditch, Phys. Rev. Lett. **52**, 2379 (1984).
[6] R. G. Della Valle and H. C. Andersen, J. Chem. Phys. **97**, 2682 (1992).
[7] D. Eisenberg and W. Kauzmann, *The Structure and Properties of Water* (Oxford University Press, New York, 1969).
[8] C. A. Angell, Annu. Rev. Phys. Chem. **34**, 593 (1983).
[9] P. G. Debenedetti, *Metastable Liquids: Concepts and Principles* (Princeton University Press, Princeton, 1996).
[10] R. J. Speedy and C. A. Angell, J. Chem. Phys. **65**, 851 (1976).
[11] G. S. Kell, J. Chem. Eng. Data **12**, 66 (1967).
[12] D. E. Hare and C. M. Sorensen, J. Chem. Phys. **84**, 5085 (1986).
[13] O. Mishima, L. D. Calvert, and E. Whalley, Nature (London) **314**, 76 (1985).
[14] O. Mishima, J. Chem. Phys. **100**, 5910 (1994).
[15] P. H. Poole, T. Grande, F. Sciortino, H. E. Stanley, and C. A. Angell, Comput. Mater. Sci. **4**, 373 (1995).
[16] M.-C. Bellissent-Funel, Europhys. Lett. **42**, 161 (1998).
[17] G. P. Johari, J. Chem. Phys. **105**, 7079 (1996).
[18] R. J. Speedy, P. G. Debenedetti, R. S. Smith, C. Huang, and B. D. Kay, J. Chem. Phys. **105**, 240 (1996).
[19] P. H. Poole, F. Sciortino, U. Essman, and H. E. Stanley, Nature (London) **360**, 324 (1992).
[20] S. H. Harrington, R. Zhang, P. H. Poole, F. Sciortino, and H. E. Stanley, Phys. Rev. Lett. **78**, 2409 (1997).
[21] H. Tanaka, Nature (London) **380**, 328 (1996).
[22] C. J. Roberts and P. G. Debenedetti, J. Chem. Phys. **105**, 658 (1996).
[23] C. J. Roberts, A. Z. Panagiotopoulos, and P. G. Debenedetti, Phys. Rev. Lett. **77**, 4386 (1996).
[24] O. Mishima and H. E. Stanley, Nature (London) **392**, 164 (1998).
[25] M. R. Sadr-Lahijany, A. Scala, S. V. Buldyrev, and H. E. Stanley, Phys. Rev. Lett. **81**, 4895 (1998).
[26] H. E. Stanley and J. Teixeira, J. Chem. Phys. **73**, 3404 (1980).
[27] Y. Xie, K. F. Ludwig, G. Morales, D. E. Hare, and C. M. Sorensen, Phys. Rev. Lett. **71**, 2050 (1993).
[28] S. Sastry, P. G. Debenedetti, F. Sciortino, and H. E. Stanley, Phys. Rev. E **53**, 6144 (1996).
[29] L.-P. Rebelo, P. G. Debenedetti, and S. Sastry, J. Chem. Phys. **109**, 626 (1998).
[30] H. Tanaka, Phys. Rev. Lett. **80**, 5750 (1998).
[31] R. J. Speedy, J. Phys. Chem. **86**, 982 (1982).
[32] P. H. Poole, F. Sciortino, T. Grande, H. E. Stanley, and C. A. Angell, Phys. Rev. Lett. **73**, 1632 (1994).
[33] C. A. Jeffery and P. H. Austin, J. Chem. Phys. **110**, 484 (1999).
[34] S. S. Borick, P. G. Debenedetti, and S. Sastry, J. Phys. Chem. **99**, 3781 (1995).
[35] R. A. Heidemann and J. M. Prausnitz, Proc. Natl. Acad. Sci. USA **73**, 1773 (1976).
[36] M. S. Wertheim, J. Stat. Phys. **35**, 35 (1984).
[37] M. S. Wertheim, J. Stat. Phys. **42**, 459 (1986).
[38] I. Nezbeda, J. Mol. Liq. **73-4**, 317 (1997), and references therein.
[39] G. Jackson, W. G. Chapman, and K. E. Gubbins, Mol. Phys. **65**, 1 (1988).
[40] W. G. Chapman, K. E. Gubbins, G. Jackson, and M. Radosz, Ind. Eng. Chem. Res. **29**, 1709 (1990).
[41] P. J. Smits, I. G. Economou, C. J. Peters, and J. D. Arons, J. Phys. Chem. **98**, 12080 (1994).
[42] I. G. Economou and M. D. Donohue, Fluid Phase Equilibria **116**, 518 (1996).
[43] L. W. Dahl and H. C. Andersen, J. Chem. Phys. **78**, 1980 (1983).
[44] T. L. Hill, *Statistical Mechanics: Principles and Selected Applications* (Dover, New York, 1987).
[45] N. F. Carnahan and K. E. Starling, J. Chem. Phys. **51**, 635 (1969).
[46] A. Papoulis, *Probability, Random Variables, and Stochastic Processes* (McGraw–Hill, New York, 1984).
[47] S. Torquato, Phys. Rev. E **51**, 3170 (1995).
[48] H. Reiss, H. L. Frisch, and J. L. Lebowitz, J. Chem. Phys. **31**, 369 (1959).
[49] H. Reiss and A. D. Hammerich, J. Phys. Chem. **90**, 6252 (1986).
[50] R. J. Speedy, J. Phys. Chem. **92**, 2016 (1988).
[51] H. Reiss, J. Phys. Chem. **96**, 4736 (1992).
[52] S. Torquato, Phys. Rev. Lett. **74**, 2156 (1995).
[53] T. M. Truskett, S. Torquato, and P. G. Debenedetti, Phys. Rev. E **58**, 7369 (1998).
[54] P. C. Hemmer and G. Stell, Phys. Rev. Lett. **24**, 1284 (1970); G. Stell and P. C. Hemmer, J. Chem. Phys. **56**, 4274 (1972); J. M. Kincaid, G. Stell, and E. Goldmark, *ibid.* **65**, 2172 (1976).
[55] P. G. Debenedetti, V. S. Raghavan, and S. S. Borick, J. Phys. Chem. **95**, 4540 (1991).
[56] D. H. Rasmussen, A. P. MacKenzie, C. A. Angell, and J. C. Tucker, Science **181**, 342 (1973).